Applied Physics A manuscript No.
(will be inserted by the editor)

Plasma-enhanced atomic-layer-deposited MoO_x emitters for silicon heterojunction solar cells

Johannes Ziegler[1], Mathias Mews[3], Kai Kaufmann[4,5], Thomas Schneider[1], Alexander N. Sprafke[1], Lars Korte[3], Ralf B. Wehrspohn[1,2⋆]

[1] Martin-Luther-University Halle-Wittenberg, *μMD Group*, Institute of Physics, Heinrich-Damerow-Strasse 4, 06120 Halle, Germany
[2] Fraunhofer Institute for Mechanics of Materials IWM Halle, Walter-Hülse-Str. 1, 06120 Halle, Germany
[3] Helmholtz-Zentrum Berlin für Materialien und Energie GmbH, Institute for Silicon-Photovoltaics, Kekuléstr. 5,12489 Berlin, Germany
[4] Fraunhofer Center for Silicon Photovoltaics CSP, Otto-Eifeld-Strasse 12, 06120 Halle, Germany
[5] Hochschule Anhalt Köthen, University of Applied Sciences, Bernburger Str. 55, 06966 Köthen

Received: date / Revised version: date

Abstract A method for the deposition of molybdenum oxide (MoO_x) with high growth rates at temperatures below 200 °C based on plasma-enhanced atomic layer deposition (PE-ALD) is presented. The stoichiometry of the of the over-stoichiometric MoO_x films can be adjusted by the plasma-parameters. First results of these layers acting as hole-selective contacts in silicon heterojunction (SHJ) solar cells are presented and discussed.

1 Introduction

Its spectrally broad transparency and high work function makes evaporated molybdenum oxide (MoO_x) a promising candidate for substituting amorphous silicon emitter in silicon heterojunction (SHJ) solar cells [1]. Thus the replacement of the p-doped amorphous silicon emitter by higher band gap materials like MoO_x can lead to a gain in the photo current of such cells[2][3]. However, a thin intrinsic amorphous silicon((i)a-Si:H) layer between the oxide and the crystalline silicon (c-Si) is still needed to improve the poor surface passivation quality of the oxide and to fully benefit of the MoO_x -induced high open circuit voltage (V_{OC}) [3].
Although the hole-selective conductivity mechanism through the MoO_x /(i)a-Si:H/(n)c-Si stack is not fully understood in detail, it is influenced by the defect state density in the MoO_x as well as the MoO_x layer thickness itself[3][4].
For depositing very thin (<10 nm), conformal oxides on structured silicon surfaces atomic layer depostion (ALD) is due to its reaction-limited growth process an ideal candidate[5].Thermal ALD recipes for MoO_x are recently reported by different groups, but up to now non of these MoO_x layers are tested as emitter alternative in SHJ solar cells[6][7][8].
In this work, we introduce an alternative new plasma enhanced atomic layer deposition (PE-ALD) process for MoO_x layers. Influences of the process conditions on the stoichiometry of these layers,as well as there performance on cell level are shown.

2 Experimental

The MoO_x deposition was carried out by an PE-ALD process in a FlexAL ALD reactor (Oxford instruments) with inductively-coupled plasma source. Before starting a deposition the reactor chamber is pumped to a base pressure below 0.7 mPa and the substrate is heated to 180°C . Due to the low vapor pressure of the used liquid Mo precursor $(NtBu)_2(NMe_2)_2Mo$, the source is heated to 50 °C and transported to the reactor chamber by Ar gas (step 1). After the first precursor dose the reactor chamber is purged by Ar only (step 2), while later in the purge step the Ar flow through the ICP source is changed to O_2 to get a stable O_2 flow trough the plasma source (step 3). In next step (step 4) O_2 plasma is burned over the substrate with a plasma power of 300 W. The last step (step 5) in the cycle is done by flowing O_2 through the ICP source for the one second (1 second O_2 plasma) and the two second O_2 (2 second O_2 plasma) plasma processes (figures: 1, 2). The minimal reactor pressure is set to 2 Pa. The upper limit of each step of the different processes is given in the process cycle overview of the processes (see figures: 1, 2, 3). The PE-ALD plasma

Send offprint requests to: Johannes Ziegler
⋆ e-mail: johannes.ziegler@physik.uni-halle.de

step duration is varied between 1 s (figure:1) and 2 s (figure:2). Additionally, the influence of an Ar plasma on the MoO_x layers is tested by inserting an six second Ar plasma step with 300 W plasma power (2 second O_2 plasma & Ar) (compare figure:3).

duration one cycle 7.2 s

	Step	max.pressure	O_2 flow
1	$C_{12}H_{30}N_4Mo$ dose	12.0 Pa	no
2	dose purge	4.0 Pa	no
3	stabilisation	2.4 Pa	yes
4	O_2 plasma	2.0 Pa	yes
5	plasma purge	4.4 Pa	yes

Fig. 1: Schema PE-ALD MoO_x process "1 second O_2 plasma".

duration one cycle 8.2 s

	Step	max.pressure	O_2 flow
1	$C_{12}H_{30}N_4Mo$ dose	16.0 Pa	no
2	dose purge	4.9 Pa	no
3	stabilisation	2.6 Pa	yes
4	O_2 plasma	2.0 Pa	yes
5	plasma purge	6.4 Pa	yes

Fig. 2: Schema PE-ALD MoO_x process "2 second O_2 plasma".

duration one cycle 13.2 s

	Step	max.pressure	O_2 flow
1	$C_{12}H_{30}N_4Mo$ dose	2.7 Pa	no
2	dose purge	2.7 Pa	no
3	stabilisation	2.6 Pa	yes
4	O_2 plasma	2.0 Pa	yes
5	plasma purge	5.4 Pa	no
6	Ar plasma	2.6 Pa	no

Fig. 3: Schema PE-ALD MoO_x process "2 second O_2 & Ar plasma".

The thicknesses and growth per cycle (GPC) of the produced MoO_x layers on silicon substrate are measured by spectral ellipsometry using a Tauc-Lorentz model combined with an Gauss oscillator to model sub band gap absorption if necessary [9]. X-ray photoelectrons spectra of the as deposited MoO_x layers are measured by a Kratos Axis Ultra photoelectrons spectrometer (x-ray source Al $E_{K_\alpha} = 1486.7$eV).

For the solar cell preparation polished float-zone grown phosphorous doped (100) silicon wafers with a resistivity of 1-5 Ωcm were used. The wafers were cleaned using the RCA process and dipped in diluted hydrofloric acid (2 min, 1 % vol.) prior to amorphous silicon depositions and 5 nm intrinsic amorphous silicon were deposited at the front side of the wafers and a stack of 4 nm intrinsic and 8 nm phosphorous-doped amorphous silicon was deposited on the back side.
Amorphous silicon layers were deposited by plasma enhanced chemical vapor deposition. The intrinsic amorphous silicon layers were deposited using an excitation frequency of 13.56 MHz and a power density of 20 mW/cm^2. The deposition temperature was 170°C, the pressure 0.5 mbar, the distance between electrode and substrate on the grounded electrode was 3 cm and the process gas consisted of pure silane. The intrinsic layers were exposed to a hydrogen plasma treatment[10] in the same reactor at 1 mbar, an electrode substrate distance of 5 cm and a plasma power density of 60 mW/cm^2.
Phosphorous-doped amorphous silicon was grown in a reactor with 60 MHz excitation, at 0.5 mbar, 195°C, with an electrode distance of 2.3 cm, at plasma power density of 20 mW/cm^2 with a gas phase doping of 2000 ppm provided by mixing phosphine diluted at 1 % in hydrogen with silane.
Directly after a 1 min dip in 1 %vol.diluted Hf, to remove an potential native oxide from the amorphous silicon, 10 and 20 nm thick molybdenum oxide layer have been deposited by the introduced PE-ALD processes with varying plasma steps on the front side of the wafers. Following the molybdenum oxide depositions indium-tin-oxide (ITO) was sputtered onto the samples. The ITO layers were RF-sputtered from a ceramic target at a pressure of 6 mbar, a sputtering power of 70 W, a voltage of about 165 V and a gas flow of 40 sccm. The sputter gas consisted of Argon with 0.2 % oxygen for the front side ITO and 0.5 % oxygen for the back side layer. The thickness of the front side ITO is about 80 nm, while about 150 nm were deposited on the back side. Since the layers were deposited at room temperature a two minute post deposition anneal at 200°C was conducted.
Metal contacts were applied by thermal evaporation of titanium silver stacks. 10 nm of titanium were deposited as an adhesion layer and 500 nm of silver were added on the back side and 1500 nm on the front side. The front side evaporation was conducted through a shadow mask. Afterwards the solar cell area of 1 cm^2 was defined by photolithography and HCl etching of the ITO layer on the front side.
Photoconductanse decay measurements were conducted using a Sinton Instruments system to measure the minority carrier lifetime of the wafers in between different process steps[11]. Bright IV of the solar cells were measured using a class c sun simulator.

3 Results and discussion

In figure 4 the MoO_x film thickness determined by spectral ellipsometry, plotted over the number of performed ALD cycles for the 1 second and 2 second O_2 plasma processes, is shown. A very similar linear increase of layer thickness with number of cycles is found for both

processes. The relatively high growth rate per cycle of 0.06(5)±0.008 nm for both O_2 plasma durations indicates that oxygen saturation is reached at a plasma power of 300 W within 1 s. This high growth rate at 180 °C is one main benefit compared to the thermal ALD MoO_x process reported by Bertuch et. al.[8], which use the same Mo precursor but ozone as oxidant.For the thermal ALD MoO_x process at temperatures below 200 °C growth rate per cycle below 0.03 nm are reported. By PE-ALD the activation energy can be delivered by the oxygen reactants from O_2 plasma. This enables higher growth rates specially for lower deposition temperatures.The growth rates are not significantly influenced by longer purge times or by the integration of an additional Ar plasma step in the cycle, like its done in process 2 second O_2 and 6 second Ar plasma (figure:3) (not shown).

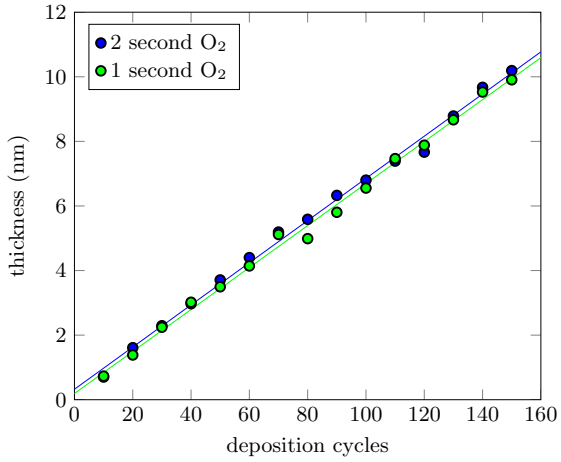

Fig. 4: MoO_x thickness measured by spectral ellipsometrie data poltted versus the number of ALD cycles.

The optical parameters, estimated from the ellipsometry data of the different MoO_x layers, are slightly affected by the duration of the plasma step (compare figure5). While the 2 second O_2 plasma process shows no sub band gap absorption the additional Argon plasma step leads to small, wide sub band gap absorption in the MoO_x layers the. For 1 second O_2 plasma duration the sub band gap absorption is more pronounced and less wide (figure5).

X-ray photoelectron spectroscopy (XPS) was used to identify the core level binding energies and oxidation states of the MoO_x layers.The spectra of the films on silicon show characteristic peaks for the oxygen molybdenum. Beside a small carbon peak from surface contamination no additional peaks can be found in the survey spectra (not shown).In figure 6 very similar spectra for all processes can be found in the Mo 3d doublet region. Two peaks are observed at 232.5 and 235.6 eV, which corresponds to the Mo $3d_{5/2}$ and Mo $3d_{3/2}$ respectively. This values are consistent with reported values for the

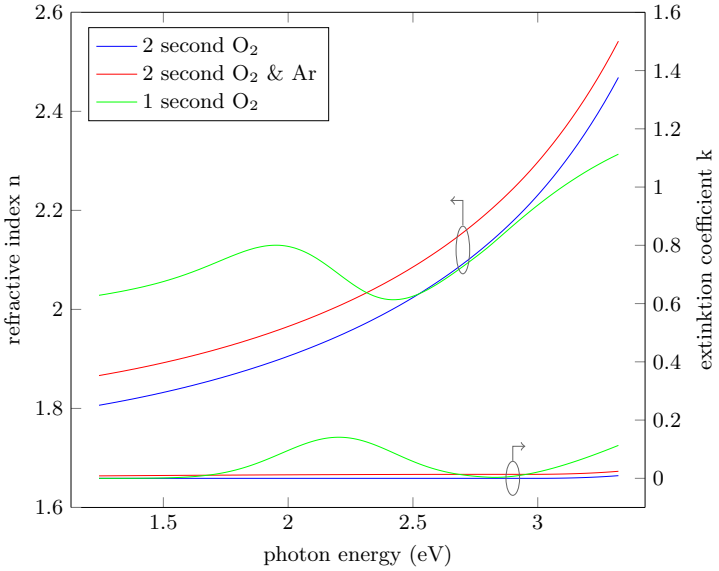

Fig. 5: Refractive index n and extinction coefficient k of the produced MoO_x layer as determined from spectroscopic ellipsometry.

Mo oxidation state of 6 + in literature(232.3 - 232.6 eV for the Mo $3d_{5/2}$ and 235.4 - 235.7 eV for the Mo $3d_{3/2}$ [4][12][8][6]).

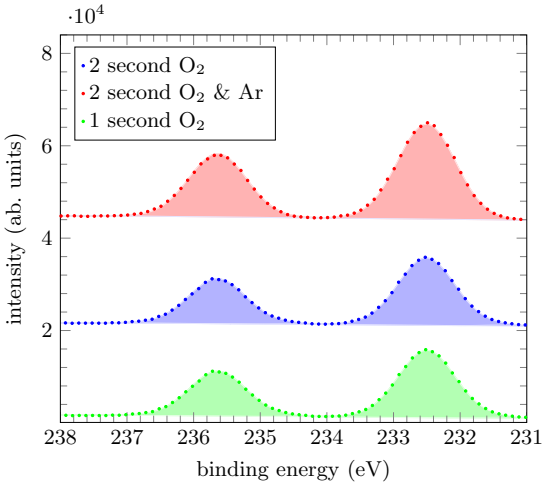

Fig. 6: XPS spectra of the Mo3d doublet of MoO_x films grown in PE-ALD processes with varying plasma step.

A clear difference can be found in the O 1s energy region in figure 7. While all measurements show a similar O 1s peak at 530.3 eV a second oxygen related peak at higher binding energies can be found in the spectra. In the 1 second O_2 process spectrum this peak at 531.3 eV is less pronounced, compared to the spectra of 2 second O_2 processes, in which this peak is located at slightly higher binding energies at 531.8 eV. Choi and coauthors [12] assign a very similar peak in molybdenum oxide

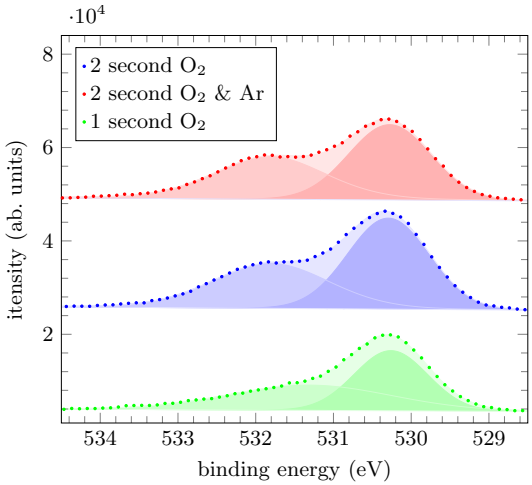

Fig. 7: XPS spectra of O1s energy region of MoO_x films grown in PE-ALD processes with varying plasma step.

to strongly absorbed oxygen as O^-, HO^- or H_2O. Although we can not exclude that this peak is formed by adsorbed air moisture in the layers, as samples were not transferred in vacuo in to the spectrometer. It is very likely that this difference are process related, in particular because the samples have been produced after each other and transfered together. It seems plausible that a longer oxygen plasma step leads to a higher content of strongly absorbed oxygen in the MoO_x layers itself. However a stoichiometry analysis of the measured XPS spectra show over-stoichiometric ($x > 3$) MoO_x for all produced layers. While the O to Mo proportion $x = 3.15$ is estimated for the 1 second O_2 layer, a higher oxygen content is measured for 2 second O_2 plasma processes $x = 3.62$ without and $x = 3.55$ with Ar plasma step.
The performance of the different MoO_x processes is tested for 10 nm and 20 nm thick oxide layers in SHJ solar cells. The cell results (compare figure 8) show significant differences mainly in the open circuit voltage. While the oxides grown in the 2 second O_2 plasma processes reach best V_{OC} values above 610 mV up to 650 mV, the best V_{OC} values reach by the oxides grown in the 1 second O_2 plasma processes are below 580 mV. It is worth to mention, that the low open circuit voltages in these cells are not limited by enhanced surface recombination. From lifetime measurements of the samples after ITO sputtering and post anneal(not shown) a quasi-Fermi level splitting at 1 sun (often called implied V_{OC}) well above 700 mV could be measured for all samples. Both process without Ar plasma step tend to slightly lower open circuit voltages for thicker oxide layer. Cells with MoO_x layers grown in a process with Ar plasma step show an opposite trend.
The parasitic absorption in the thin oxides is not the only optical loss, shadowing of the ITO itself, as well as differences in the reflection of the front side stacks are also limiting the current. Therefor the cells with thin (10 nm) oxide layers show very similar currents. A loss in current by doubling the oxide thickness can be seen in all produced cells. As expected the 1 s O_2 plasma processed MoO_x layers show the highest optical lose, by doubling the layer thickness, above 1.3 mA cm^{-2}. Although the extinction coefficient, determined by spectral ellipsometry on as deposited oxide layers, are slightly higher for the MoO_x process with Ar plasma step the short circuit currents do not reflect such tendencies. This could indicate that the ITO sputtering step and the post deposition anneal determines the optical properties of the MoO_x layers. The fill factors and efficiency of all cells are

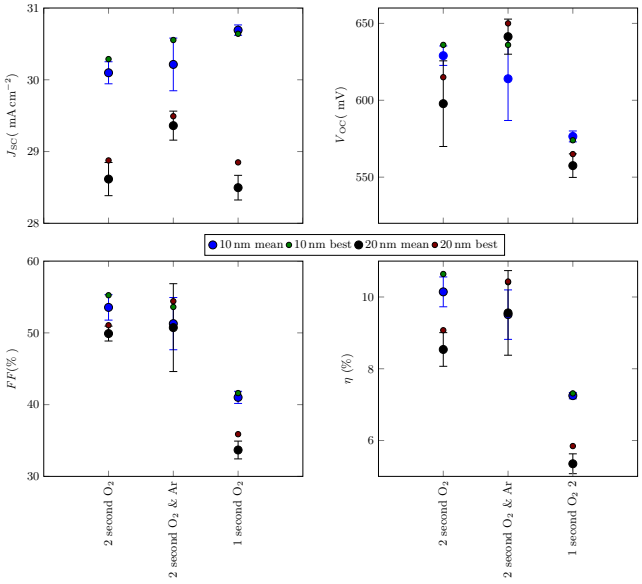

Fig. 8: Solar cell results versus MoO_x processes for 10 nm and 20 nm thick oxide layers

limited by differently strong pronounced s-shape in the bright IV curves(compare figures 10 and 11). Bataglia et. al. [3] have reported similar "s-shape" feature, more pronounced for thicker evaporate MoO_x layers of SHJ solar cells with MoO_x emitter. Same tendencies can be found here for cells with MoO_x layers grown in PE-ALD process without additional Ar plasma step. One possible reason for such shape could be the existence of a large barrier for hole transport in SHJ solar cells with sufficient front surface passivation [13]. At first sight it seems plausible to assume that an insufficient hole transport through the MoO_x layers itself is the dominating part of such barrier in the produced cells. The decrease in fill factor for thicker oxide layer seems to supporting this idea. Anyhow MoO_x layers grown in PE-ALD process with additional Ar plasma step do not show such dependence. On the other hand the valence band offset on the a-Si:H/c-Si interface could bee the dominating part of the barrier, if a tunneling process of holes through this offset is dominating the current a wider barrier leads to a more pronounced s-shape. The wide of such barrier

is working point dependent and directly influenced by the band bending. A lower work-function of the MoO_x would introduce an lower dark band bending in the c-Si (see schematic sketch in figure 9).

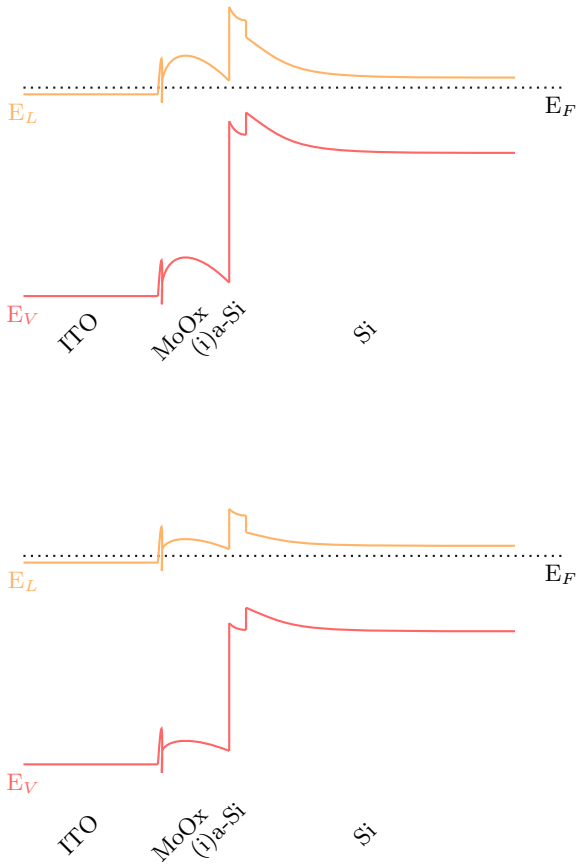

Fig. 9: Sketch illustrating differences in MoO_x induced dark band bending above: high work-function MoO_x , below: low work-function MoO_x .

Therefore a lower open circuit voltage, and as well a more pronounced "s-shape" can be expected. In total it leads to a significant loss in fill factor and efficiency
It is known that work-function in sub-stoichiometric molybdenum oxide($x < 3$) decrease by the removal of oxygen [14]. Although all as deposited oxides are over-stoichiometric we speculate that the ITO sputter step and the post deposition anneal can reduce the oxygen content in the MoO_x layers during the cell process. It might be somehow plausible that after these reduction the MoO_x layers with initial less oxygen still have a lower content and therefore a lower work function compared to layers with higher initial oxygen content. Such an effect would explain the high decrease in V_{OC} and fill factor seen in cells with MoO_x layers grown the 1 second O_2 PE-ALD process, with lower initial oxygen content.

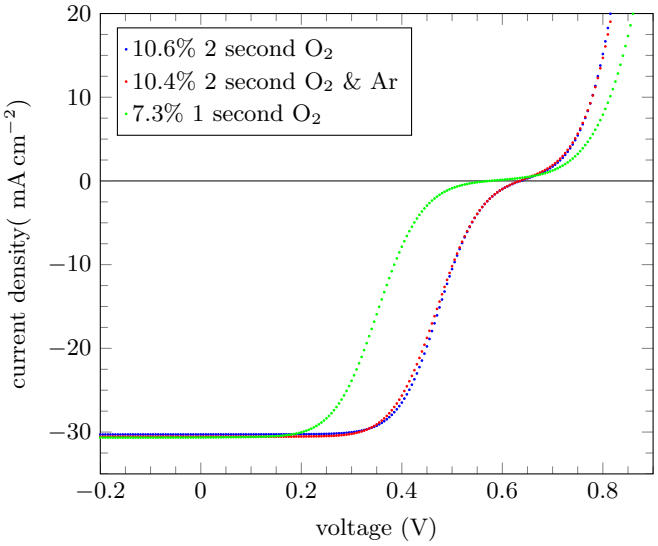

Fig. 10: Bright IV-curves of SHJ cells with 10 nm MoO_x .

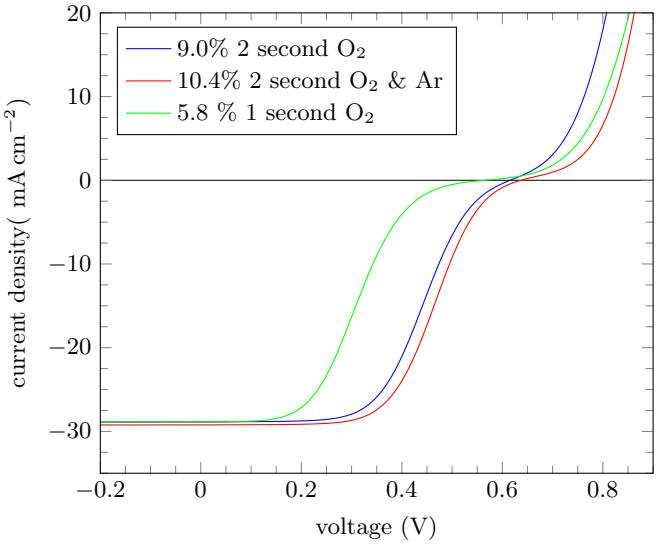

Fig. 11: Bright IV-curves of SHJ cells with 20 nm MoO_x .

4 Conclusions

A new PE-ALD process for the deposition of MoO_x with high growth rate at temperatures below 200 °C has been presented. XPS measurements show that the stoichiometry of the grown oxides can be influenced by the duration of the oxidizing plasma step. In a first experiment the

integration of this MoO_x layers as alternative emitters in SHJ solar cells are tested with efficiencies above 10 %. A strong influence of initial stoichiometry on the open circuit voltage and on cell performance can be reported. The best cells have a 10 nm MoO_x layer and a 2 second oxygen plasma step.

Acknowledgements The authors would like to thank Kerstin Jacob and Mona Wittig for wafer cleaning. Financial support was provided by the European Commission through the FP7-ENERGY Project HERCULES (Grant Agreement No. 608498) and from the German Federal Ministry of Education and Research (BMBF) within the research college STRUKTURSOLAR.

References

1. C. Battaglia, X. Yin, M. Zheng, I.D. Sharp, T. Chen, S. McDonnell, A. Azcatl, C. Carraro, B. Ma, R. Maboudian, R.M. Wallace, A. Javey, Nano Letters **14**(2), 967 (2014). DOI 10.1021/nl404389u. URL http://dx.doi.org/10.1021/nl404389u. PMID: 24397343
2. T. Mueller, S. Schwertheim, M. Scherff, W.R. Fahrner, Applied Physics Letters **92**(3), 033504 (2008). DOI http://dx.doi.org/10.1063/1.2837192. URL http://scitation.aip.org/content/aip/journal/apl/92/3/10.1063/1.2837192
3. C. Battaglia, S.M. de Nicols, S. De Wolf, X. Yin, M. Zheng, C. Ballif, A. Javey, Applied Physics Letters **104**(11), 113902 (2014). DOI http://dx.doi.org/10.1063/1.4868880. URL http://scitation.aip.org/content/aip/journal/apl/104/11/10.1063/1.4868880
4. M.T. Greiner, L. Chai, M.G. Helander, W.M. Tang, Z.H. Lu, Advanced Functional Materials **23**(2), 215 (2013). DOI 10.1002/adfm.201200993. URL http://dx.doi.org/10.1002/adfm.201200993
5. M. Otto, M. Kroll, T. Kasebier, R. Salzer, A. Tunnermann, R.B. Wehrspohn, Appl. Phys. Lett. **100**(19), 191603 (2012). DOI 10.1063/1.4714546. URL http://link.aip.org/link/?APL/100/191603/1
6. M. Diskus, O. Nilsen, H. Fjellvag, J. Mater. Chem. **21**, 705 (2011). DOI 10.1039/C0JM01099E. URL http://dx.doi.org/10.1039/C0JM01099E
7. Y.C. Tseng, A.U. Mane, J.W. Elam, S.B. Darling, Solar Energy Materials and Solar Cells **99**(0), 235 (2012). DOI http://dx.doi.org/10.1016/j.solmat.2011.12.004. URL http://www.sciencedirect.com/science/article/pii/S0927024811006854. 9th International Meeting on Electrochromism
8. A. Bertuch, G. Sundaram, M. Saly, D. Moser, R. Kanjolia, Journal of Vacuum Science & Technology A **32**(1), 01A119 (2014). DOI http://dx.doi.org/10.1116/1.4843595. URL http://scitation.aip.org/content/avs/journal/jvsta/32/1/10.1116/1.4843595
9. G.E. Jellison, F.A. Modine, Applied Physics Letters **69**(14), 2137 (1996). DOI http://dx.doi.org/10.1063/1.118155. URL http://scitation.aip.org/content/aip/journal/apl/69/14/10.1063/1.118155
10. M. Mews, T.F. Schulze, N. Mingirulli, L. Korte, Appl. Phys. Lett. **102**, 122106 (2013). DOI 10.1063/1.4798292
11. R. Sinton, A. Cuevas, M. Stuckings, Proc. of the 25th IEEE PVSC pp. 457 –460 (1996)
12. J.G. Choi, L. Thompson, Applied Surface Science **93**(2), 143 (1996). DOI http://dx.doi.org/10.1016/0169-4332(95)00317-7. URL http://www.sciencedirect.com/science/article/pii/0169433295003177
13. U. Das, S. Hegedus, L. Zhang, J. Appel, J. Rand, R. Birkmire, in *Photovoltaic Specialists Conference (PVSC), 2010 35th IEEE* (2010), pp. 001,358–001,362. DOI 10.1109/PVSC.2010.5614372
14. M.T. Greiner, L. Chai, M.G. Helander, W.M. Tang, Z.H. Lu, Advanced Functional Materials **22**(21), 4557 (2012). DOI 10.1002/adfm.201200615. URL http://dx.doi.org/10.1002/adfm.201200615